A coherently stimulated Brillouin spectrometer

Joel N. Johnson,[1,2,*] Co Authors,[3] and Ryan O. Behunin[1,2,†]

[1] *Department of Applied Physics and Materials Science, Northern Arizona University, Flagstaff, AZ, 86011, USA*
[2] *Center for Materials Interfaces in Research and Applications, Northern Arizona University, Flagstaff, AZ, 86011, USA*
[3] *Department, Address*

(Dated: October 29, 2024)

We present a novel coherently stimulated Brillouin spectrometer utilizing a detuned pump-probe design that exploits a relaxation of phase-matching requirements at small lengths, enabling room temperature traveling-wave phonon spectroscopy at the micrometer scale with sub-10 femtowatt sensitivity. This approach surpasses the limitations of traditional stimulated Brillouin techniques. Our instrument's sensitivity was validated using 1 cm of UHNA3 fiber and 100 micrometers of bulk carbon disulfide liquid, demonstrating its capability to measure Brillouin scattering in materials with low Brillouin gain or, with particular advantage, small effective lengths. This advancement opens new possibilities for nanometer-scale Brillouin spectroscopy and the development of nano-acousto-optic devices.

I. INTRODUCTION

Brillouin scattering, the inelastic interaction between light and acoustic phonons, is a fundamental phenomenon used to probe the mechanical and structural properties of materials at microscopic scales. In spontaneous Brillouin scattering, thermally excited acoustic phonons scatter incident light, resulting in frequency shifts that reveal information about the material's elastic properties and acoustic modes. However, the weak signal inherent to spontaneous Brillouin scattering often necessitates long acquisition times and limits spatial resolution, posing challenges for high-resolution material characterization.

Stimulated Brillouin scattering (SBS) enhances this interaction by using intense optical fields to amplify the acoustic wave through a nonlinear optical process. In SBS, a strong pump laser interacts with a counter-propagating Stokes wave, leading to the generation of coherent acoustic phonons via electrostriction. The resulting interference reinforces the acoustic wave, which in turn scatters more light from the pump into the Stokes frequency, creating a positive feedback loop. This amplification allows for more efficient excitation and detection of acoustic phonons, enabling applications in optical signal processing, sensing, and high-resolution spectroscopy [1].

However, conventional SBS techniques face notable limitations when probing small volumes or samples with low Brillouin gain. The strict phase-matching conditions required for efficient SBS typically demand interaction lengths on the order of centimeters to meters, restricting spatial resolution and making it challenging to study micro- and nanoscale systems. Additionally, separating the pump and scattered signals often requires complex optical filtering due to their close spectral proximity, complicating the experimental setup.

To overcome these challenges, various approaches have been explored. Techniques utilizing optical cavities enhance the interaction by increasing the effective interaction length, but they require precise alignment and are sensitive to environmental fluctuations [2]. Forward Brillouin scattering methods, such as those demonstrated by Kittlaus et al., are advantageous in applications requiring relaxed phase-matching conditions, albeit at the cost of increased modal complexity [3]. Coherent probe beam amplification schemes have been proposed to improve sensitivity, yet they can introduce additional noise and complexity, as phase noise in laser sources can lead to significant gain fluctuations and performance penalties [4].

In this work, we present a coherently stimulated Brillouin spectrometer that employs a detuned pump-probe scheme to relax the phase-matching requirements at small interaction lengths. By introducing a separate probe laser detuned from the pump, we achieve coherent amplification of the acoustic wave without the need for strict phase matching over long distances. This design allows for the separation of the probe and pump frequencies, simplifying signal detection and filtering.

Our approach enables room-temperature traveling-wave phonon spectroscopy at the micrometer scale with sub-10 femtowatt sensitivity, surpassing the limitations of traditional SBS techniques. We demonstrate the capabilities of our instrument by measuring Brillouin scattering in 1 centimeter of ultrahigh numerical aperture (UHNA3) fiber and 100 micrometers of bulk carbon disulfide liquid. These measurements highlight the instrument's ability to characterize materials with low Brillouin gain or small effective lengths.

The development of this coherently stimulated Brillouin spectrometer opens new avenues for nanometer-scale Brillouin spectroscopy and facilitates the character-

* joel.johnson@nau.edu
† ryan.behunin@nau.edu

ization and development of nano-acousto-optic devices. It holds promise for advancing research in material science, photonics, and sensing technologies, where high spatial resolution and sensitivity are paramount, marking a significant step toward practical, room-temperature Brillouin-based spectroscopy and sensing solutions.

II. THEORETICAL FRAMEWORK

Coherently stimulated four-wave Brillouin scattering

Stimulated Brillouin scattering (SBS), illustrated by the schematic in Fig. 1(a) for the Stokes process, is a three-wave mixing process in which incident pump laser light of frequency ω_{Pump} inelastically scatters from a traveling-wave phonon of frequency Ω to produce light that is frequency-shifted by the phonon frequency. In the Stokes process the phonon is retreating from the incident laser light and the scattered light is shifted down in frequency ($\omega_{Stokes} = \omega_{Pump} - \Omega$). Light scattered in the backwards direction spatially overlaps with the incident laser light, allowing the two optical fields interfere to produce a frequency at the difference between the two ($\omega_{Pump} - \omega_{Stokes}$). Since this difference frequency is exactly equal to the frequency of the acoustic field Ω, the beating of the incident pump light and the backscattered Stokes light produces an electrostrictive reinforcement of the acoustic wave. This driving of the acoustic wave in turn increases the scattering rate of the incident pump light, producing a positive feedback process and an exponential increase of the amplitude of the backscattered Stokes wave.

Fig. 1(b) shows the schematic of coherently stimulated four-wave Brillouin scattering for the Stokes process. We introduce a dedicated external Stokes laser of frequency ω_{Stokes} that strongly drives the electrostrictive reinforcement of the acoustic field in the material. The backscattered Stokes light which is normally collected in an SBS process to infer mechanical properties of the material is now drowned out by the much higher power external Stokes laser. To resolve this, we introduce an additional external laser at a distinct frequency ω_{Probe} which copropagates with the pump laser and backscatters in the material from the strongly driven acoustic field. This produces a backscattered signal to be collected ($\omega_{Signal} = \omega_{Probe} - \Omega$) which is distinguishable from the high-powered Stokes laser light.

To quantify the performance of this setup, we derive the coupled-wave equations for the four-wave mixing process. These equations describe the relationship between the optical fields and the acoustic field in the material. The full derivation can be found in Appendix A, where the scattered power of the backscattered signal is shown to be

$$P_{Sig} = \frac{1}{4}(G_B L)^2 P_P P_S P_{Pr} sinc^2\left(\frac{\Delta k L}{2}\right), \qquad (1)$$

where P_P, P_S, and P_{Pr} are the powers of the pump, Stokes, and probe lasers, respectively, and G_B is the effective Brillouin gain,

$$G_B = \frac{g_0}{A_{eff}} \frac{\left(\frac{\Gamma_B}{2}\right)^2}{(\Omega - \Omega_B)^2 + \left(\frac{\Gamma_B}{2}\right)^2}, \qquad (2)$$

with the on-resonance gain factor of the material given by

$$g_0 = \frac{\gamma_e^2 \omega^2}{n v c^3 \rho_0 \Gamma_B}. \qquad (3)$$

Here, γ_e is the electrostrictive constant, ω is the pump frequency, n is the refractive index of the material, v is the sound speed of the material, c is the speed of light, ρ_0 is the mean density of the material, and Γ_B is the Brillouin linewidth, or dissipation rate, of the material. In Eq. 2, Ω_B is the resonant Brillouin frequency of the material, A_{eff} is the effective area of the material, Δk is the wavevector mismatch between the optical fields, to be discussed next, and L is the effective length of the material.

Phase matching relaxation

In all nonlinear optical processes, efficiency is maximized when phase matching conditions are satisfied. A frequency mismatch (energy unconservation) or a wavevector mismatch (momentum unconservation) each result in drastically reduced efficiency of a given process.[5] This can be seen by Eq. 1, where the wavevector mismatch, Δk, is contained within a $sinc^2$ function. This $sinc^2$ term thereby defines the phase matching bandwidth of the system, notably scaling with effective interaction length L.

We apply this wavevector mismatch allowance to the pump and probe waves ($\Delta k = k_{Pump} - k_{Probe}$) so that the backscattered signal is different than the applied Stokes wave. This choice allows for selection of the signal and rejection of the Stokes with a bandpass filter, as will be discussed later. Expressed in terms of wavelengths, this gives

$$\Delta k = \frac{4\pi n \Delta\lambda}{\lambda_{Pump}\lambda_{Probe}} \approx \frac{4\pi n \Delta\lambda}{\lambda_{Pump}^2}. \qquad (4)$$

We can apply this to the phasematching bandwidth term to find the fraction of maximum scattered power, Φ, that can be expected for a given L and phase mismatch $\Delta\lambda$ between the pump and probe,

$$\Phi \equiv sinc^2\left(\frac{2\pi n \Delta\lambda L}{\lambda_{Pump}^2}\right). \qquad (5)$$

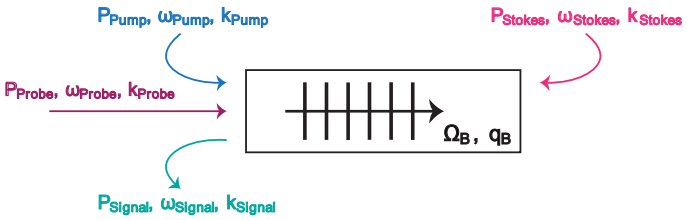

FIG. 1. Illustration of 4-Wave Brillouin Scattering.

Using this expression for Φ, we see that for an effective length of one meter a wavelength mismatch of only 0.6 pm from 1.55 μm pump light in UHNA3 fiber drops the scattered power to one half of maximum. However, for shorter effective lengths the wavevector mismatch becomes more forgiving; a 36 pm mismatch preserves 82.5% of the maximum signal for a length of 1 cm and all else equal. This separation, translating to about 4.5 GHz, is meaningful, as it represents sufficient spectral separation for the backscattered signal to be isolated from the applied Stokes light.

Further, for even smaller lengths, Eq. 5 gives an increase in the fraction of the maximum signal produced, given equivalent wavelength mismatch between pump and probe, because the $sinc^2$ function is sampled closer to its peak center. Alternatively, as length decreases, the probe may be further detuned from the pump and still achieve the same fraction of the maximum signal as for longer lengths, perhaps offering a slight advantage in noise reduction. It should be noted that the scattered power, as given by Eq. 1, scales with the square of the effective length. Thus, while smaller lengths allow for the ability to capture a larger fraction of this maximum scattered power, the actual amount of scattered power decreases dramatically as length decreases.

III. METHODS

Instrument design

The design of the instrument is shown in the schematic in Fig. 2. A Pump and Stokes wave is synthesized from a single tunable laser source for coherent stimulation of a sample. The Pump wave (ω_{Pump}) is amplified by an erbium-doped fiber amplifier (EDFA) and passed through a variable optical attenuator (VOA) for power control. The output is then polarization-controlled to reflect at a polarizing beam splitter (PBS) for injection into the sample. For Stokes synthesis, an AC signal (Ω) is supplied to an intensity modulator (IM) with carrier frequency nulled and a tunable filter is used to select the lower-frequency Stokes side band ($\omega_{Pump} - \Omega$). This Stokes light is then amplified by an EDFA, passed through a VOA, and polarization-controlled to reflect at a second PBS for couter-propagation to the Pump through the sample.

A separate tunable laser ($\omega_{Probe} = \omega_{Pump} + \Delta k$) is used to supply a probe wave and local oscillator (LO). Probe light is amplified by an EDFA and passed through a VOA and a polarization controller aligns the polarization for transmission through the first PBS whereby it copropagates with the Pump to be incident on the sample. Backscattered light exits the sample and transmits back through the first PBS, whereas the orthogonally polarized Stokes light reflects at this same point to be diverted to a tap for power monitoring. The backscattered Signal ($\omega_{Signal} = \omega_{Probe} + \Omega$) then routes through two subsequent circulators for spectral filtering by a 5 GHz bandpass tunable filter. This filter allows the desired backscattered Signal to pass while rejecting any reflected Probe light as well as any reflected, transmitted, or backscattered light from the Pump or Stokes waves that was not already diverted by the PBS.

The filtered Signal then heterodynes via a 99-1 splitter with the LO ($\omega_{LO} = \omega_{Probe} + \omega_{AOM}$), which is frequency-upshifted by an acousto-optic modulator (AOM) and controlled to be copolarized with the Signal. Of the resulting frequencies from the heterodyne process, only the subtracted frequency term is considered, as all others are beyond the range of detection. This heterodyned signal ($\omega_{signal} = \Omega + \omega_{AOM}$) is then captured by a photodiode detector and heterodyned again by a radio frequency (RF) mixer with a second AC signal ($\Omega + \omega_{AOM} - \omega_{Lock}$), where ω_{Lock} is a fixed-frequency under 50 MHz to be collected by a lock-in amplifier set to this fixed-frequency. ω_{Lock} is passed through a 50 MHz low-pass filter and amplified by an RF amplifier before collection. ω_{Lock} remains fixed in frequency because both AC signals involve Ω and sweep syncronously through a range under measurement.

Experimental Techniques

Here we detail some of the experimental techniques, design choices, and specific device settings which we have found optimize the signal-to-noise (SNR) of our mea-

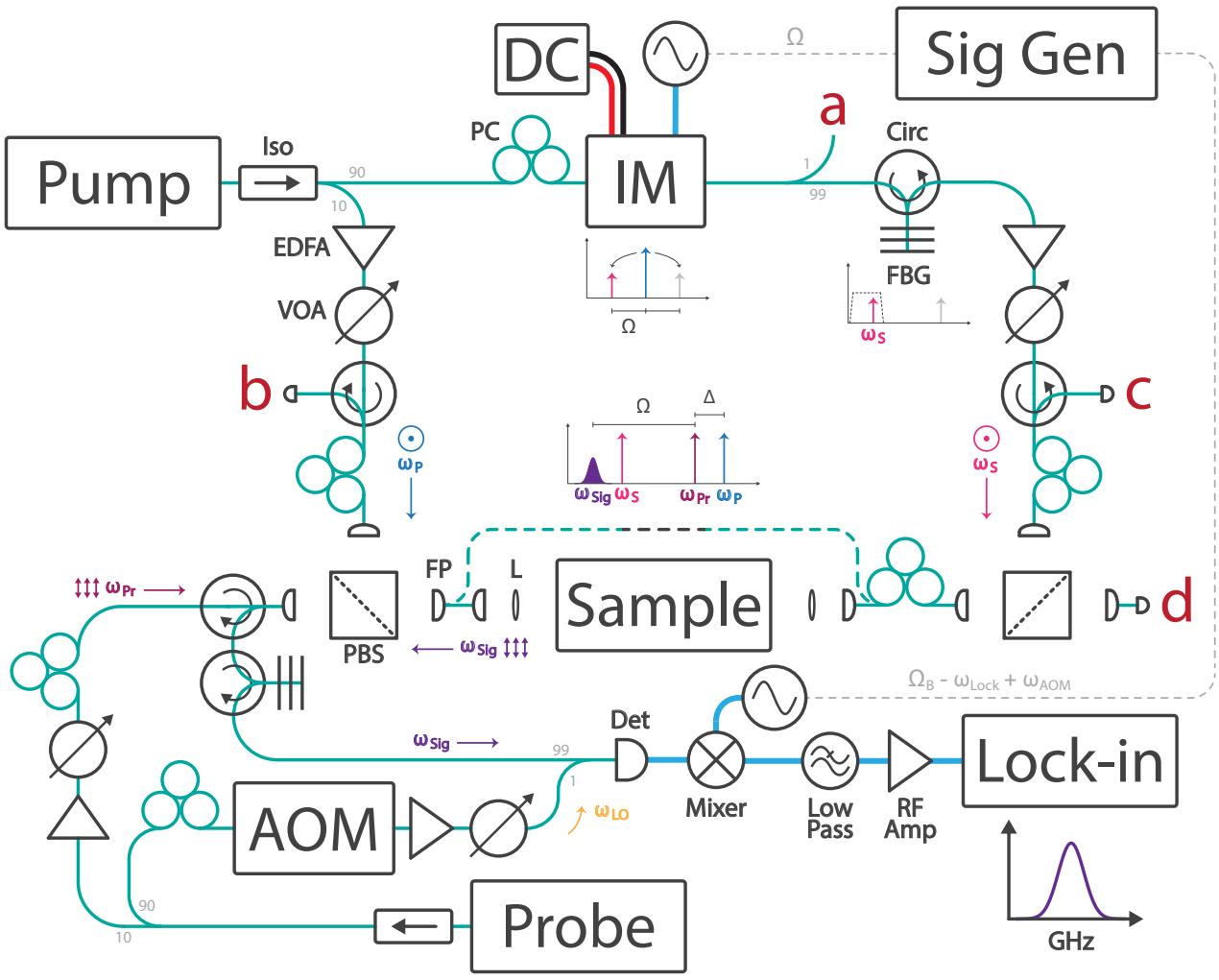

FIG. 2. Design schematic of a coherently stimulated phonon spectrometer. A tunable CW laser at approximately 1.55 μm emits light that passes through an isolator (Iso) and a splitter, diverting 10% to a 27 dBm EDFA followed by a variable optical attenuator (VOA). This Pump light (ω_P) is polarization-controlled to reflect off a polarizing beam splitter (PBS) and is recoupled to fiber via a fiber port (FP), then directed to the sample either by direct fiber coupling or through a pair of FPs and lenses (L) for free-space samples. After passing through the sample, the Pump light traverses a corrective polarization controller that mitigates fiber twists and bends before reflecting off a second PBS, where it is routed to port (c) for power monitoring. To synthesize the Stokes wave, a 90% split from the original Pump is processed through an intensity modulator (IM) and a fiber Bragg grating (FBG), generating a Stokes sideband downshifted from the Pump by Ω. This frequency shift is swept via a signal generator to capture Ω_B. A 99/1 splitter provides a tap at port (a) to optimize Stokes synthesis. The Stokes wave (ω_S), amplified by a 1 W EDFA and VOA-controlled, counter-propagates along the Pump path and is monitored at port (b). A second tunable CW laser, detuned from the Pump, generates the Probe wave (ω_{Pr}), which is amplified by a 1 W EDFA, attenuated variably, and polarization-controlled to pass through the initial PBS where it is incident on the sample. Backscattered Signal light (ω_{sig}) transmits back through the PBS, while unscattered Probe light transmits to a power meter at port (d). A circulator parts the Signal from the Probe path, with an FBG filtering out any unwanted noise or Stokes light. Finally, the Signal is heterodyned with an EDFA-amplified, AOM-shifted local oscillator (LO) derived from the Probe laser and directed to a photodiode for detection. The resulting RF signal is mixed with an AC LO supplied by the signal generator which sweeps synchronously with the Stokes synthesis frequency, and collected by a lock-in amplifier for data processing.

surements with the instrument. Our experimental setup generates the Pump, Stokes, and Probe optical fields required for coherently stimulated Brillouin scattering. The Pump laser emits approximately 45 mW of power, of which 10% is split and amplified to approximately 0.5 W to become the Pump optical field. The other 90% of power emitted from the Pump laser is shifted to become the Stokes optical field and is amplified to approximately 1 W. Similarly, the Probe laser emits approximately 45 mW of power, of which 10% is split and amplified to approximately 1 W to become the Probe optical field and the remaining 90% is used as the LO. A 99/1 splitter was specifically chosen over a more common 50/50 splitter to heterodyne the signal and LO in order to minimize loss of the backscattered signal before being collected by the detector, as this preserves 99% of the signal power at no cost if the LO is amplified by 50x. Thus, in our setup the LO is amplified to approximately 230 mW prior to combining with the signal, resulting in the maximum allowable input power for our detector of $<$2.4 mW to be incident at the detector. Post-detector, the electronic signal is mixed with a 17 dbm AC signal and amplified by a 23 dbm RF amplifier before it is collected by a lock-in amplifier. For all measurements, it was found that setting both Pump and Probe lasers to emit in whisper mode (as opposed to dither) dramatically improves the spectral density and SNR of the measurement.

Proper matching of the demodulator settings of our Zurich Instruments HF2LI 50 MHz lock-in amplifier to the signal input is critical for maximizing the SNR of the measurement. Clock timing is synced between the signal generater and the lock-in amplifier with a 10 MHz reference signal output from the signal generator and fed into the lock-in amplifier set to accept this reference clock signal. The input signal range, which defines the gain of the analog input amplifier, should exceed the incoming signal by roughly a factor two including a potential DC offset. This is best chosen by selecting the auto feature within the lock-in software interface, which automatically adjusts the range according to a rolling 100 ms window of the maximum measured input signal amplitude. The coupling mode is set to AC, which inserts a high-pass filter that rejects DC components of the input signal, and the input impedance is set to 1MΩ. We set the low-pass filter order to the 8th order, which sets the filter to roll off at the maximum 48 dB/oct, and the data sampling rate of the input signal is set to the maximum 1.84 million Sa/s.

The SNR of a measurement is further optimized when the low-pass filter bandwidth for the lock-in amplifier input signal is minimized to match the frequency linewidth and thermally-driven variability or random drift of the incoming signal, ω_{Lock}. While the linewidth of the signal is sub-hertz, the range within which it drifts is dependent on the stability of instrument components and is typically on the order of tens of hertz. We find this frequency drift of the input signal to be less than 100 Hz after all components of the system reach equilibrium temperature (approximately 30 minutes) and thus set the low-pass filter bandwidth to 100 Hz for long measurements of a few hours. For shorter measurements of less than 15 minutes this bandwidth can typically be reduced to as little as 40 Hz without risking the signal drifting out of range.

In addition to the signal linewidth being defined by this slight signal variability just discussed, the input signal frequency is also affected by the thermally-driven variations in precision of the electronic components. The mean frequency of the incoming signal, ω_{Lock}, must precisely match the frequency that the lock-in amplifier expects to recieve, as specified in its control parameters. Achieving maximum precision requires that the frequency difference between the two output signals of the signal generator, $\omega_{Ch1} = \Omega$ and $\omega_{Ch2} = \Omega - \omega_{Lock} + \omega_{AOM}$, precisely match the lock-in frequency specified for the lock-in amplifier. This presents a challenge because, while Ω is directly controlled to subhertz precision by the signal generator, ω_{AOM} varies according to the precision of our AOM device with nominal temperature fluctuations. Despite efforts to thermally ground the device for stability, our AOM has been found to initially shift its input signal by its specified value of 40 MHz, before gradually increasing its applied shift over approximately 30 minutes as the internal components of the device warm to equilibrium operating temperature. Once at thermal equilibrium, however, the device maintains a stable shift of the signal by 40,000,820 Hz $\pm$ 50 Hz, allowing for a stable mean lock-in frequency and a relatively narrow filter bandwidth of 100 Hz to capture the variability contribution of the AOM.

IV. RESULTS

Instrument sensitivity

We begin by testing the sensitivity of the instrument as a way of defining a performance metric for the instrument which can be used to indicate what material, power, and length combinations might be possible to measure. From Eq. 1, the sensitivity of the instrument is the minimum scattered power, P_{Signal}, to produce a statistically significant measurement. To determine this, we target a specific length, L, of a sample of known effective Brillouin gain, G_B. We keep the pump-probe detuning, $\Delta\lambda$, constant across measurements and record the pump, Stokes, and probe optical powers to calculate the scattered power. Starting with sufficient optical powers to produce a clearly distinguishable measurement, we gradually reduce the optical powers until the sensitivity floor is reached.

To serve as our sensitivity testbed, we prepared 1 cm of Nufern's UHNA3 fiber, a well-studied fiber with known effective Brillouin gain[6]. Additionally, UHNA3 fiber offers several properties that make it ideal for this task of unambiguous detection of the Brillouin signal as it diminishes with each subsequent reduction in optical powers.

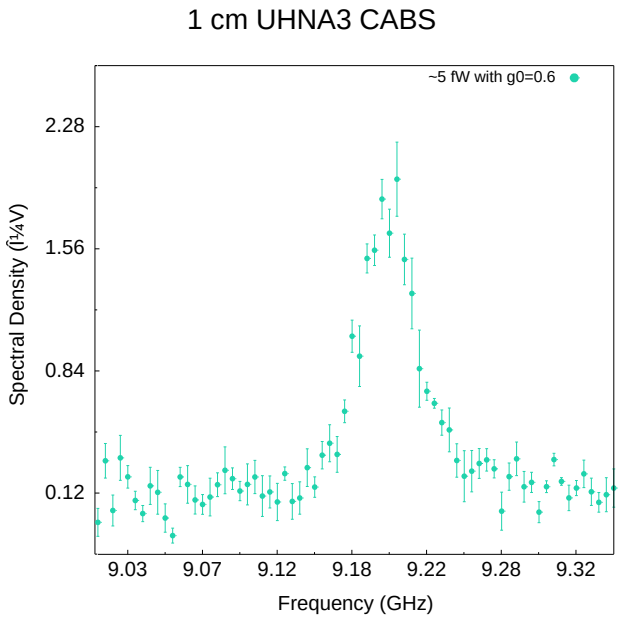

FIG. 3. 5 fW sensitivity measurement

First, it offers a Brillouin shift that is spectrally far from that of the single-mode fiber (SMF28) which constitutes much of the instrument. This ensures that the Brillouin response of the sample is not conflated with the Brillouin response of the instrument itself. Additionally, the core of UHNA3 fiber features a high concentration of germanium which improves the optical and acoustic guidance in the fiber as a result of the large refractive index difference between core and cladding. Finally, UHNA3 fiber offers a high optomechanical nonlinear response, with an effective Brillouin gain of 0.6 $W^{-1}m^{-1}$ measured at room temperature[6]. This gain factor is larger than that of SMF28 by an order of magnitude[7].

The Brillouin signal corresponding to a sensitivity of $P_{Signal} = 5\,\mathrm{fW}$ is shown in Fig. 3. The data represent an average of five consecutive measurements, from which an average of five consecutive background measurements has been subtracted. Error bars indicate the 1σ standard deviation of the mean, also known as the standard error. The measurement appears to offer an SNR greater than 5, estimated by visually comparing the peak spectral density at the center frequency to the spectral density off resonance. Assuming a normal noise distrubution profile, an SNR of 5 is equivalent to a 5σ confidence interval, or 99.7% confidence in the statistical significance of this measurement. This characterization of the sensitivity of our instrument provides the essential information needed to assess the feasibility of more challenging measurements going forward, such as those involving materials with low Brillouin gain or samples with small effective lengths. Relevant parameters used for this measurement and calculation of on-resonance scattered power are listed in Table I.

G_B $(W^{-1}m^{-1})$	L (m)	P_P (μW)	P_S (μW)	P_{Pr} (mW)	$\Delta\lambda$ (pm)
0.6	0.01	506	504	2.01	20

TABLE I. Measurement parameters for sensitivity measurement and calculation.

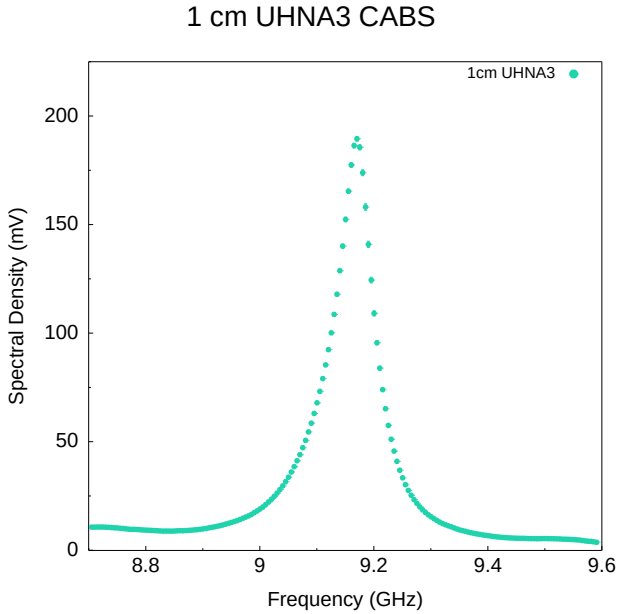

FIG. 4. 1cm UHNA3

Measurements

We demonstrate the capabilities of the instrument on the two most common classes of samples: fiber and bulk material. For a fiber sample we again choose UHNA3 for its higher nonlinear response and excellent optical and acoustic guidance. In contrast to the sensitivity measurements, we now seek to demonstrate the full measuring capabilities of the instrument and so apply all available optical power (about 1.5 W) to maximize the backscattered signal from the sample. We target the same 1 cm segment of UHNA3 fiber as was used for determining sensitivity.

Fig. 4 shows the spectral profile captured for 1 cm of UHNA3 fiber, revealing the expected lorentzian profile consistent with Eq. 2. The peak amplitude of the spectra occurs at 9.1704 GHz, indicating the Brillouin resonance frequency of the longitudinal traveling-wave mode in the fiber. The FWHM of the measurement is 80 MHz and provides a measure of the phonon dissipation rate. Both values match what is seen in the literature for SBS measurements of UHNA3 fiber.[6] The data shown are a background-subtracted average of five successive measurements taken over 10 minutes with error bars corresponding to 1σ of the standard deviation of the mean, or standard error.

To achieve this measurement of UHNA3 fiber, the instrument design was altered to include only fiber-coupled

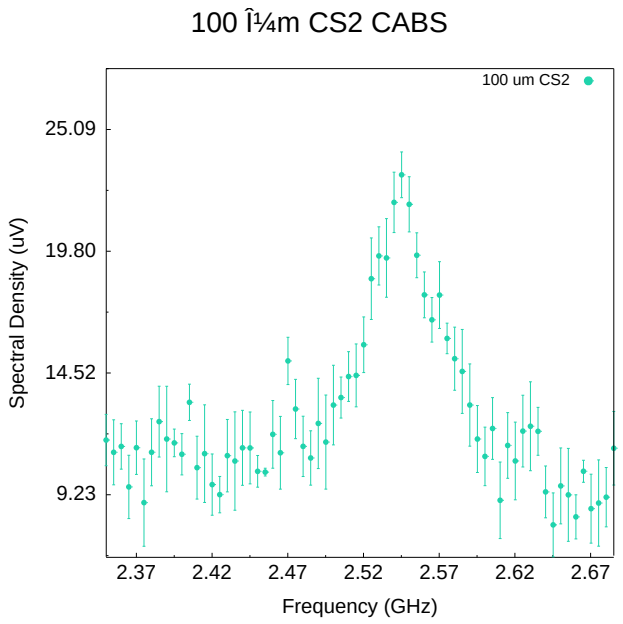

FIG. 5. 100μm CS2

segments connecting the fiber ports between the two PBSs. The pump laser wavelength was set to 1549.000 nm and the probe laser wavelength was set to 1549.020 nm, giving a frequency mismatch of approximately 2.5 GHz. The pump-probe mismatch is chosen to be only as large as needed to allow the edge of the pass-band of the probe filter to split the backscattered pump and probe light, thus rejecting any backscattered light from the pump laser and accepting only the backscattered signal from the probe laser. The Stokes filter was placed at 1549.073 nm, an offet of approximately 9.18 GHz from the pump laser to capture the Stokes sideband from the intensity modulator. This corresponds to the center of the measured frequency range and was chosen to allow the Stokes sideband output from the intensity modulator to remain within the pass band of the Stokes filter as the RF signal fed to the intensity modulator is swept through the full measurement range. The probe filter was set to 1549.109 nm, an offset of approximately 11.18 GHz from the probe laser, to capture the Stokes-shifted backscattered signal from the probe. The center frequency of the backscattered signal is of course shifted 9.18 GHz from the probe laser, however an extra offset of 2 GHz is chosen for improved rejection of any pump light as the pass band of our filter extends approximately 2.5 GHz on either side of center.

For a free-space bulk example we target carbon disulfide liquid for its exceptionally high Brillouin gain factor of 1.5 m/GW.[1] Figure 5 reveals the Brillouin signal of carbon disulfide liquid contained in a 100 μm path length cell. To our knowledge, measurement of Brillouin scattering at this scale has not been reported in the literature. A scattered power comparison would reveal that achieving such a measurement using traditional SBS techniques would require excessively high optical powers or cooling the material to cryogenic temperatures, which, of course, would be prohibitive for carbon disulfide in the liquid state.

For this measurement of carbon disulfide, the pump and probe laser wavelengths were set to 1548.808 nm and 1548.898 nm, respectively. The short path length of the sample significantly broadens Φ, the $sinc^2$ term defining the phasematching bandwidth, allowing for further separation of the pump and probe wavelengths for improved signal isolation without significant reduction in scattered power of the signal produced in the carbon disulfide. Specifically, the additional pump-probe wavelength separation of 70 pm employed for this measurement compared to the UHNA3 measurement results in a negligible 0.045% reduction in scattered power. This additional separation contributes meaningfully, however, to improved rejection of pump light by the probe filter and thus higher SNR of the signal.

Placement of the Stokes filter is critical for measurements of materials that give small Brillouin shifts, such as with carbon disulfide's 2.55 GHz shift. We offset our 5GHz bandwidth Stokes filter an additional 2 GHz to ensure the nearby carrier signal and anti-Stokes sideband from the intensity modulator are rejected and only the Stokes sideband is allowed to pass. For the measurement shown in Fig. 5, this corresponds to a Stokes and probe filter placement of 1548.844 nm and 1548.934 nm, respectively.

Phase Matching Bandwidth

We performed an additional experiment to characterize the phase matching tolerance of the instrument for a given length of sample. In this experiment, we performed a series of measurements of 1 cm of UHNA3 at constant optical powers while increasing the detuning of pump and probe lasers. From Eq. 1, this experiment holds G_B, L, P_P, P_S, and P_{Pr} constant while letting Δk vary. We expect the amplitudes of these measurements to trace out a $sinc^2$ function as given by Eq. 5. Fig. 6 shows the result of this experiment which includes 75 measurements performed between 5 GHz and 42 GHz pump-probe frequency separation, at 0.5 GHz intervals, with the peak amplitude of each measurement represented by a point. The theoretical $sinc^2$ function for the parameters used in the experiment is shown on the plot with a solid red line.

V. CONCLUSION

In conclusion, we have introduced a coherently stimulated Brillouin spectrometer utilizing a detuned pump-probe design to achieve high sensitivity and room-temperature operation in micrometer-scale samples. This approach successfully overcomes the spatial resolution limitations imposed by conventional SBS methods,

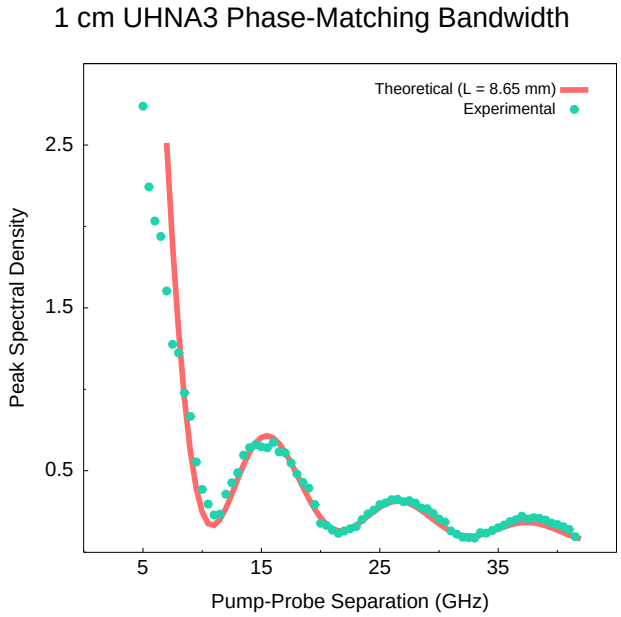

FIG. 6. Phase-matching $sinc^2$ func

demonstrating sub-10 femtowatt sensitivity in UHNA3 fiber and enabling Brillouin measurements in bulk liquid carbon disulfide with unprecedented efficiency. By relaxing phase-matching constraints, this instrument opens new possibilities for characterizing nanoscale material properties and developing nano-acousto-optic devices in standard laboratory settings without the need for cryogenic environments. Moving forward, our methodology could facilitate advancements in high-resolution phonon spectroscopy and inspire further innovations in the study of material mechanics at the microscale, reinforcing the broader applicability of Brillouin-based techniques across materials science, photonics, and sensing technologies.

ACKNOWLEDGMENTS

Appendix:

A Coherently Stimulated Brillouin Spectrometer

Appendix A: Coupled-Wave Equations

Here we derive the coupled wave equations that describe coherent stimulated Brillouin scattering involving a pump, Stokes, probe, and backscattered optical field given respectively by

$$\tilde{E}_P(z,t) = A_P e^{i(k_P z - \omega_P t)} + c.c. \tag{A1}$$

$$\tilde{E}_S(z,t) = A_S e^{i(k_S z - \omega_S t)} + c.c. \tag{A2}$$

$$\tilde{E}_{Pr}(z,t) = A_{Pr} e^{i(k_{Pr} z - \omega_{Pr} t)} + c.c. \tag{A3}$$

$$\tilde{E}_{Sig}(z,t) = A_{Sig} e^{i(k_{Sig} z - \omega_{Sig} t)} + c.c. \tag{A4}$$

and a common acoustic field given by

$$\tilde{\rho}(z,t) = \rho_0 + \rho(z,t) e^{i(qz - \Omega t)} + c.c., \tag{A5}$$

where $\Omega = \omega_P - \omega_S$ and $q = k_P - k_S = 2k_P$.

1. Acoustic Field

As in the case of SBS [1], we start by assuming that the material obeys the acoustic wave equation,

$$\frac{\partial^2 \tilde{\rho}}{\partial t^2} - \Gamma' \nabla^2 \frac{\partial \tilde{\rho}}{\partial t} - v_s^2 \nabla^2 \tilde{\rho} = \nabla \cdot \vec{f}, \tag{A6}$$

where v_s is the sound speed in the material and Γ' is a damping parameter given by

$$\Gamma' = \frac{1}{\rho}\left[\frac{4}{3}\eta_s + \eta_b + \frac{\kappa}{C_p}(\gamma - 1)\right], \tag{A7}$$

where η_s and η_b are the shear and bulk viscosity coefficients of the material, respectively. The source term on the right side of Eq. (A6) is the divergence of the electrostrictive force:

$$\vec{f} = \nabla p_{st} = \nabla \cdot \left[-\frac{1}{2}\epsilon_0 \gamma_e \Big(\langle \tilde{E}_P \cdot \tilde{E}_S \rangle + \langle \tilde{E}_{Pr} \cdot \tilde{E}_{Sig} \rangle \Big) \right] \tag{A8}$$

which yields, after applying the slowly varying amplitude approximation,

$$\nabla \cdot \vec{f} = \epsilon_0 \gamma_e q^2 (A_P A_S^* + A_{Pr} A_{Sig}^*) e^{i\Delta k z}, \tag{A9}$$

Where $\Delta k = (k_{Pr} - k_{Sig}) - (k_P - k_S)$ is the phase mismatch between the four optical fields. Only two electrostrictive

terms survive terms after accounting for the orthogonal polarization of the pump and Stokes fields with respect to that of the probe and backscattered signal. Inserting this electrostrictive force term and the acoustic field (Eq. (A5)) into Eq. (A6) and assuming a slowly varying acoustic amplitude we find

$$-2i\Omega\frac{\partial\rho}{\partial t}-\Gamma' 2iq^2\Omega\rho-2iqv_s^2\frac{\partial\rho}{\partial z}=\epsilon_0\gamma_e q^2(A_P A_S^*+A_{Pr}A_{Sig}^*)e^{i\Delta kz}, \tag{A10}$$

which can be restated in terms of the Brillouin linewidth, $\Gamma_B = q^2\Gamma'$, as

$$-2i\Omega\frac{\partial\rho}{\partial t}-2i\Omega\Gamma_B\rho-2iqv_s^2\frac{\partial\rho}{\partial z}=\epsilon_0\gamma_e q^2(A_P A_S^*+A_{Pr}A_{Sig}^*)e^{i\Delta kz}. \tag{A11}$$

Given the phonon dispersion relations $\Omega_B = |q_B|v_s$ and $\Omega^2 = q^2\left(v^2 - i\Omega\Gamma'\right)$, Eq. (A11) can be rewritten as

$$-2i\Omega\frac{\partial\rho}{\partial t}+\left(\Omega^2-\Omega^2-i\Omega\Gamma_B\right)\rho-2iqv_s^2\frac{\partial\rho}{\partial z}=\epsilon_0\gamma_e q^2(A_P A_S^*+A_{Pr}A_{Sig}^*)e^{i\Delta kz}. \tag{A12}$$

We take the common assumption that the phonon propagation distance is small compared to the distance over which the source term varies significantly, which allows the spatial derivative term in Eq. (A12). We further assume steady-state conditions such that the time derivative term also vanishes, leaving

$$(\Omega_B^2-\Omega^2-i\Omega\Gamma_B)_\rho=\epsilon_0\gamma_e q^2(A_P A_S^*+A_{Pr}A_{Sig}^*)e^{i\Delta kz}. \tag{A13}$$

We thus find the acoustic field amplitude to be

$$\rho(z,t)=\epsilon_0\gamma_e q^2\frac{(A_P A_S^*+A_{Pr}A_{Sig}^*)e^{i\Delta kz}}{\Omega_B^2-\Omega^2-i\Omega\Gamma_B}. \tag{A14}$$

2. Optical Fields

We now turn to the spatial evolution of the optical fields, described by the wave equation,

$$\frac{\partial^2\tilde{E}_i}{\partial z^2}-\frac{n^2}{c^2}\frac{\partial^2\tilde{E}_i}{\partial t^2}=\frac{1}{\epsilon_0 c^2}\frac{\partial^2\tilde{P}_i}{\partial t^2}, \tag{A15}$$

where i denotes the four optical fields, namely: pump, Stokes, probe, and backscattered signal. The total nonlinear polarization that gives rise to the source term in the wave equation is given by

$$\tilde{P}=\epsilon_0\Delta\chi\tilde{E}=\epsilon_0\Delta\epsilon\tilde{E}=\epsilon_0\rho^{-1}\gamma_e\tilde{\rho}\tilde{E}. \tag{A16}$$

The parts of $\tilde{P}$ that can act as phase-matched source terms for the optical fields are

$$\tilde{P}_P=p_P e^{i(k_P z-\omega_P t)}+c.c.=\frac{1}{2}\epsilon_0\rho_0^{-1}\gamma_e\rho A_S e^{i(k_P z-\omega_P t)} \tag{A17}$$

$$\tilde{P}_S=p_S e^{i(-k_S z-\omega_S t)}+c.c.=\frac{1}{2}\epsilon_0\rho_0^{-1}\gamma_e\rho^* A_P e^{i(-k_S z-\omega_S t)} \tag{A18}$$

$$\tilde{P}_{Pr} = p_{Pr}e^{i(k_{Pr}z-\omega_{Pr}t)} + c.c. = \frac{1}{2}\epsilon_0\rho_0^{-1}\gamma_e\rho A_{Sig}e^{i(k_{Pr}z-\omega_{Pr}t)}e^{i\Delta kz} \tag{A19}$$

$$\tilde{P}_{Sig} = p_{Sig}e^{i(-k_{Sig}z-\omega_{Sig}t)} + c.c. = \frac{1}{2}\epsilon_0\rho_0^{-1}\gamma_e\rho^* A_{Pr}e^{i(-k_{Sig}z-\omega_{Sig}t)}e^{-i\Delta kz}. \tag{A20}$$

Inserting the optical fields (Eqs. A1-A4) and phase-matched source terms (Eqs. A17-A20) into Eq. (A15), we obtain

$$\frac{\partial A_P}{\partial z} + \frac{n}{c}\frac{\partial A_P}{\partial t} = \frac{i\omega_P\gamma_e}{2nc\rho_0}\rho A_2 \tag{A21}$$

$$-\frac{\partial A_S}{\partial z} + \frac{n}{c}\frac{\partial A_S}{\partial t} = \frac{i\omega_S\gamma_e}{2nc\rho_0}\rho^* A_P \tag{A22}$$

$$\frac{\partial A_{Pr}}{\partial z} + \frac{n}{c}\frac{\partial A_{Pr}}{\partial t} = \frac{i\omega_{Pr}\gamma_e}{2nc\rho_0}\rho A_{Sig} \tag{A23}$$

$$-\frac{\partial A_{Sig}}{\partial z} + \frac{n}{c}\frac{\partial A_{Sig}}{\partial t} = \frac{i\omega_{Sig}\gamma_e}{2nc\rho_0}\rho^* A_{Pr} \tag{A24}$$

We again assume steady-state conditions, allowing the time derivative term to be dropped. Plugging in the acoustic field amplitude (Eq. A14), we arrive at the coupled-amplitude wave equations for the optical fields,

$$\frac{\partial A_P}{\partial z} = \frac{i\epsilon_0\omega_P q^2\gamma_e^2}{2nc\rho_0}\frac{(A_P|A_S|^2 + A_{Pr}A_{Sig}^* A_S)e^{i\Delta kz}}{\Omega_B^2 - \Omega^2 - i\Omega\Gamma_B} \tag{A25}$$

$$\frac{\partial A_S}{\partial z} = -\frac{i\epsilon_0\omega_S q^2\gamma_e^2}{2nc\rho_0}\frac{(|A_P|^2 A_S^* + A_{Pr}A_{Sig}^* A_P)e^{-i\Delta kz}}{\Omega_B^2 - \Omega^2 + i\Omega\Gamma_B} \tag{A26}$$

$$\frac{\partial A_{Pr}}{\partial z} = \frac{i\epsilon_0\omega_{Pr} q^2\gamma_e^2}{2nc\rho_0}\frac{(A_P A_S^* A_{Sig} + A_{Pr}|A_{Sig}|^2)e^{i\Delta kz}}{\Omega_B^2 - \Omega^2 - i\Omega\Gamma_B} \tag{A27}$$

$$\frac{\partial A_{Sig}}{\partial z} = -\frac{i\epsilon_0\omega_{Sig} q^2\gamma_e^2}{2nc\rho_0}\frac{(A_P A_S^* A_{Pr} + |A_{Pr}|^2 A_{Sig}^*)e^{-i\Delta kz}}{\Omega_B^2 - \Omega^2 + i\Omega\Gamma_B} \tag{A28}$$

We drop the very small signal amplitude terms on the right side of Eqs. A25-A28 and integrate each along the effective length to get the amplitudes,

$$A_P = \frac{i\epsilon_0\omega_P q^2\gamma_e^2}{2nc\rho_0}\frac{A_P|A_S|^2}{\Omega_B^2 - \Omega^2 - i\Omega\Gamma_B}\frac{e^{i\Delta kL} - 1}{i\Delta k}, \tag{A29}$$

$$A_S = -\frac{i\epsilon_0\omega_S q^2\gamma_e^2}{2nc\rho_0}\frac{|A_P|^2 A_S^*}{\Omega_B^2-\Omega^2+i\Omega\Gamma_B}\frac{e^{-i\Delta kL}-1}{-i\Delta k}, \tag{A30}$$

$$A_{Pr} = \frac{i\epsilon_0\omega_{Pr} q^2\gamma_e^2}{2nc\rho_0}\frac{A_P A_S^* A_{Sig}}{\Omega_B^2-\Omega^2-i\Omega\Gamma_B}\frac{e^{i\Delta kL}-1}{i\Delta k}, \tag{A31}$$

$$A_{Sig} = -\frac{i\epsilon_0\omega_{Sig} q^2\gamma_e^2}{2nc\rho_0}\frac{A_P A_S^* A_{Pr}}{\Omega_B^2-\Omega^2+i\Omega\Gamma_B}\frac{e^{-i\Delta kL}-1}{-i\Delta k}. \tag{A32}$$

We focus on the signal amplitude given by Eq. A32, noting that close to resonance, the denomenator of the middle term containing Ω can be approximated as,

$$\Omega_B^2-\Omega^2+i\Omega\Gamma_B \approx \Omega_B(\Omega-\Omega_B+i\Gamma_B) \tag{A33}$$

giving

$$A_{Sig} = -\frac{i\epsilon_0\omega_{Sig} q^2\gamma_e^2}{2nc\rho_0}\frac{A_P A_S^* A_{Pr}}{\Omega_B(\Omega-\Omega_B+i\Gamma_B)}\frac{e^{-i\Delta kL}-1}{-i\Delta k}, \tag{A34}$$

and in fact on resonance the expression reduces to

$$A_{Sig} = -\frac{i\epsilon_0\omega_{Sig} q^2\gamma_e^2}{2nc\rho_0}\frac{A_P A_S^* A_{Pr}}{\Omega_B i\Gamma_B}\frac{e^{-i\Delta kL}-1}{-i\Delta k}. \tag{A35}$$

Remembering that $q = 2k_P = 2\omega n/c$ and also that $q = \Omega_B/v_s$, we can express the leading terms as

$$A_{Sig} = -\frac{\epsilon_0\omega^2\gamma_e^2}{c^2 v_s\rho_0\Gamma_B}A_P A_S^* A_{Pr}\frac{e^{-i\Delta kL}-1}{-i\Delta k}, \tag{A36}$$

where we have dropped the signal designator on ω. Defining g_0, as Boyd does, as

$$g_0 = \frac{\gamma_e^2\omega^2}{nvc^3\rho_0\Gamma_B}, \tag{A37}$$

reduces this expression to

$$A_{Sig} = -\epsilon_0 ncg_0 A_P A_S^* A_{Pr}\frac{e^{-i\Delta kL}-1}{-i\Delta k}. \tag{A38}$$

The intensity of the backscattered signal is given by the magnitude of the time-averaged Poynting vector, given by

$$I_i = 2n\epsilon_0 c|A_i|^2, \qquad i = 1,2,3, \tag{A39}$$

which produces for the signal intensity

$$I_{Sig} = 2\epsilon_0 nc(\epsilon_0 ncg_0)^2 |A_P|^2 |A_S^*|^2 |A_{Pr}|^2 \left| \frac{e^{-e\Delta kL} - 1}{-i\Delta k} \right|^2 = 2\epsilon_0^3 \epsilon_0 n^3 c^3 g_0^2 \frac{I_P}{2\epsilon_0 nc} \frac{I_S}{2\epsilon_0 nc} \frac{I_{Pr}}{2\epsilon_0 nc} \left| \frac{e^{-e\Delta kL} - 1}{-i\Delta k} \right|^2. \quad \text{(A40)}$$

The squared modulus term containing Δk can be reduced as

$$\left| \frac{e^{-i\Delta kL} - 1}{-i\Delta k} \right|^2 = \frac{(e^{-i\Delta kL} - 1)(e^{i\Delta kL} - 1)}{(\Delta k)^2} = \frac{L^2}{(\Delta kL)^2} \left[2 - 2\left(\frac{e^{i\Delta kL} + e^{-1\Delta kL}}{2} \right) \right]$$

$$= \frac{2L^2(1 - cos\Delta kL)}{(\Delta kL)^2} = \frac{4L^2 sin^2\left(\frac{\Delta kL}{2}\right)}{\left(\Delta kL\right)^2} = \frac{L^2 sin^2\left(\frac{\Delta kL}{2}\right)}{\left(\frac{\Delta kL}{2}\right)^2} = L^2 sinc^2\left(\frac{\Delta kL}{2}\right) \quad \text{(A41)}$$

giving as a final expression for backscattered signal intensity,

$$I_{Sig} = \frac{1}{4}(g_0 L)^2 I_P I_S I_{Pr} sinc^2\left(\frac{\Delta kL}{2}\right). \quad \text{(A42)}$$

To find the power of the backscattered signal, we would integrate this intensity over the effective area. For a uniform area A_{eff}, this gives

$$P_{Sig} = I_{Sig} A_{eff} = \frac{1}{4}(g_0 L)^2 \frac{A_{eff}}{A_{eff}} I_P \frac{A_{eff}}{A_{eff}} I_S \frac{A_{eff}}{A_{eff}} I_{Pr} sinc^2\left(\frac{\Delta kL}{2}\right) A_{eff} \quad \text{(A43)}$$

or,

$$P_{Sig} = \frac{1}{4}(G_B L)^2 P_P P_S P_{Pr} sinc^2\left(\frac{\Delta kL}{2}\right), \quad \text{(A44)}$$

where,

$$G_B = \frac{g_0}{A_{eff}}. \quad \text{(A45)}$$

We can also see that off resonance, the Ω term from Eq. A34 goes to a lorentzian form after taking the squared modulus for intensity.

Appendix B: Pump, Stokes, and Probe Contribute Equally

Equation (1) verifies the somewhat counterintuitive result that the powers of the Pump, Stokes, and Probe waves contribute equally to the scattered power of the Signal. Initially, this experiment was motivated by a practical consideration: we had obtained an amplifier with significantly greater amplification than the others and we wanted to determine if its placement on any specific line (Pump, Stokes, or Probe) would offer any advantage over another.

To test this, we conducted a controlled experiment with a 1 mm carbon disulfide (CS_2) sample. For each measurement, one of the three source powers (Pump, Stokes, or Probe) was systematically reduced by 75% while holding the others constant, ensuring consistent experimental conditions across trials. The table below shows the respective powers for each source during the three measurements, along with the multiplicative total of the three powers for each measurement.

Measurement	**Pump Power (mW)**	**Stokes Power (mW)**	**Probe Power (mW)**	**Total (mW^3)**
Pump Lower	19.190	32.210	54.560	3.372×10^4
Stokes Lower	76.600	8.020	54.650	3.359×10^4
Probe Lower	76.600	32.530	13.480	3.359×10^4

TABLE II. Power values for each source (Pump, Stokes, Probe) across the three measurements, with the multiplicative total power for each setup.

Figure 7 displays the average results from these three measurements, plotted with error bars representing one standard deviation of the mean. For increased certainty, Figure 8 presents the same data with error bars extended to two standard deviations, providing additional confidence in the reproducibility of the results.

This experiment confirmed that the scattered Signal power indeed depends equally on each of the three contributing wave powers, as expected from the theoretical framework. Consequently, the placement of the amplifier does not impact the Signal power, allowing flexibility in its use across any of the three lines. This result reinforces the reliability of Equation (1) for predicting Signal power across a range of power distributions within practical settings.

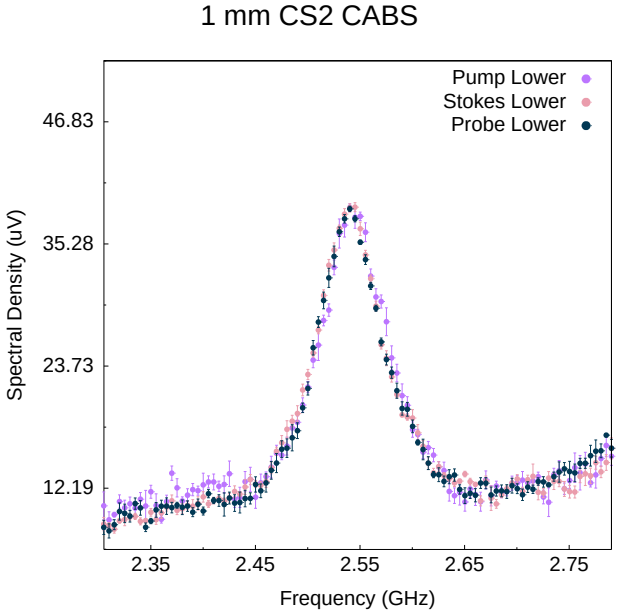

FIG. 7. 1sigma

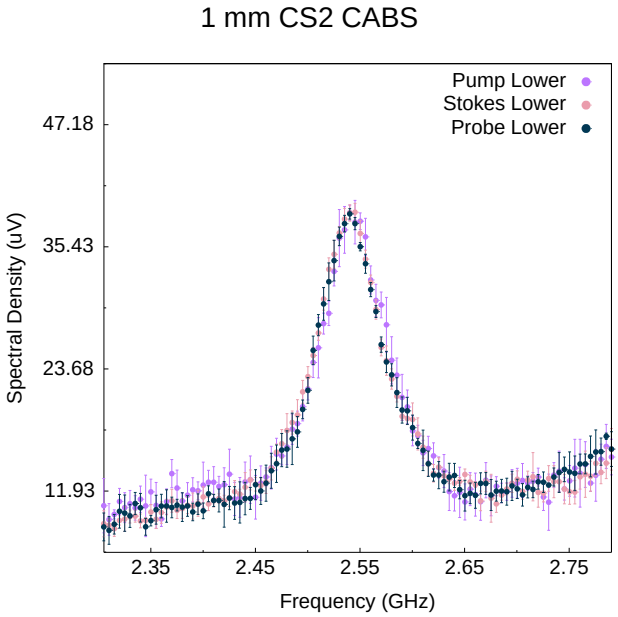

FIG. 8. 2sigma

Appendix C: Comparison to SBS

1. 1 Centimeter UHNA3 Scattered Power

2. 100 Micrometers CS2 Scattered Power

Appendix D: Alternative Configurations

1. Mirrored Design

2. Forward Scattering

3. Radial Modes

4. Shear Modes

5. Torsional Modes

6. Coherent Raman Spectroscopy

[1] R. W. Boyd, *Nonlinear Optics* (Academic Press, 2020).
[2] R. Pant, E. Li, D.-Y. Choi, C. Poulton, S. J. Madden, B. Luther-Davies, and B. J. Eggleton, Cavity enhanced stimulated brillouin scattering in an optical chip for multiorder stokes generation, Optics letters **36**, 3687 (2011).
[3] E. A. Kittlaus, N. T. Otterstrom, and P. T. Rakich, On-chip inter-modal brillouin scattering, Nature communications **8**, 15819 (2017).
[4] O. Shlomovits, T. Langer, and M. Tur, The effect of source phase noise on stimulated brillouin amplification, Journal of Lightwave Technology **33**, 2639 (2015).
[5] P. Maker, R. Terhune, M. Nisenoff, and C. Savage, Effects of dispersion and focusing on the production of optical harmonics, Physical review letters **8**, 21 (1962).
[6] R. Behunin, P. Kharel, W. Renninger, H. Shin, F. Carter, E. Kittlaus, and P. Rakich, Long-lived guided phonons in fiber by manipulating two-level systems, arXiv preprint arXiv:1501.04248 (2015).
[7] M. Nikles, L. Thevenaz, and P. A. Robert, Brillouin gain spectrum characterization in single-mode optical fibers,

Journal of Lightwave Technology **15**, 1842 (1997).